Journal of Pharmaceutical Analysis 11 (2021) 422–434

Contents lists available at ScienceDirect

Journal of Pharmaceutical Analysis

journal homepage: www.elsevier.com/locate/jpa

Original article

Biocompatible silver nanoparticles: An investigation into their protein binding efficacies, anti-bacterial effects and cell cytotoxicity studies

Sourav Das [a], Leader Langbang [b], Mahabul Haque [a], Vinay Kumar Belwal [c], Kripamoy Aguan [b], Atanu Singha Roy [a, *]

[a] Department of Chemistry, National Institute of Technology Meghalaya, Shillong, 793003, India
[b] Department of Biotechnology & Bioinformatics, North-Eastern Hill University, Shillong, 793022, India
[c] Department of Bioscience and Bioengineering, Indian Institute of Technology Guwahati, Assam, 781039, India

ARTICLE INFO

Article history:
Received 7 April 2020
Received in revised form
27 November 2020
Accepted 1 December 2020
Available online 8 December 2020

Keywords:
Green tea
Polyphenols
Silver nanoparticles
Anti-bacterial
Cytotoxicity
Hen egg white lysozyme (HEWL)

ABSTRACT

Green synthesis of silver nanoparticles (AgNPs) has garnered tremendous interest as conventional methods include the use and production of toxic chemicals, products, by-products and reagents. In this regard, the synthesis of AgNPs using green tea (GT) extract and two of its components, (−)-epigallocatechin gallate (EGCG) and (+)-catechin (Ct) as capping/stabilizing agents, is reported. The synthesized AgNPs showed antibacterial activity against the bacterial strains *Staphylococcus aureus* and *Escherichia coli*, along with anticancer activity against HeLa cells. After administering nanoparticles to the body, they come in contact with proteins and results in the formation of a protein corona; hence we studied the interactions of these biocompatible AgNPs with hen egg white lysozyme (HEWL) as a carrier protein. Static quenching mechanism was accountable for the quenching of HEWL fluorescence by the AgNPs. The binding constant (K_b) was found to be higher for EGCG-AgNPs ($(2.309 \pm 0.018) \times 10^4\ M^{-1}$) than for GT-AgNPs and Ct-AgNPs towards HEWL. EGCG-AgNPs increased the polarity near the binding site while Ct-AgNPs caused the opposite effect, but GT-AgNPs had no such observable effects. Circular dichroism studies indicated that the AgNPs had no such appreciable impact on the secondary structure of HEWL. The key findings of this research included the synthesis of AgNPs using GT extract and its constituent polyphenols, and showed significant antibacterial, anticancer and protein-binding properties. The −OH groups of the polyphenols drive the in situ capping/stabilization of the AgNPs during synthesis, which might offer new opportunities having implications for nanomedicine and nanodiagnostics.

1. Introduction

At present, nanobiotechnology, which is a combination of nanotechnology, biotechnology, chemical processing, material science, and system engineering, is one of the fastest developing research areas. The use of nanoparticles (NPs), especially gold and silver, in commercial and medicinal applications, has rapidly increased within the last decade due to their fascinating properties and intriguing applications, such as biosensing, medical imaging, cancer nanomedicine, and paints [1–5]. Conventional techniques, routes, and methodologies used for the synthesis of these nanoparticles have come under scrutiny due to the use or production of hazardous chemicals, products, by-products, reagents and solvents [6,7]. Therefore, greener and more eco-friendly techniques are being investigated for nanoparticle synthesis worldwide, using plant and fruit extracts [8], bacteria [9], fungi [10], yeast [11], and algae [12]. Green chemistry provides an environmentally compatible scheme for the fabrication of functional metal NPs [13,14]. Recently, polyphenols obtained from plants, fruits, and vegetables [15] have garnered interest for the synthesis of metal NPs [13,16–18].

Green tea (GT) is a common beverage worldwide, and its physicochemical properties and bioactive properties, such as its anti-cancer [19] and anti-inflammatory activities [20], and for the treatment of diseases such as dementia and Alzheimer's disease have been well investigated [21]. The worldwide annual consumption of GT is approximately 600,000 tons, which accounts for about 1/5 of all kinds of tea consumed [22]. GT contains bioactive

Peer review under responsibility of Xi'an Jiaotong University.
* Corresponding author.
E-mail addresses: singharoyatanu@gmail.com, asroy86@nitm.ac.in (A. Singha Roy).

https://doi.org/10.1016/j.jpha.2020.12.003

polyphenols, which are collectively referred to as catechins, accounting for about 80%–90% of the polyphenol content and approximately 40% of the total water-soluble solids [23]. The chemical structures of the major catechins found in GT are depicted in Fig. 1 [24]. Recently, tea polyphenols and other polyphenols have been used to synthesize various NPs [25,26], which were further screened for their antibacterial effects [18], cytotoxicity, anti-cancer effects, lipopolysaccharide-induced inflammatory response in microglial cells [16,20,27,28], and nanoparticle-protein interactions [29].

From a biological and medicinal point of view, the principal interest in nanoparticle is rooted in the concept that due to their relatively small size, they can communicate with cellular machinery and possibly enter previously inaccessible target locations, such as the brain [30,31]. Therefore, when looking at the potential in vivo applications of NPs, the recognition and control of these nanoparticle-protein interactions in the bloodstream are of prime importance. There are several hundreds of proteins in the human biological system that would constantly compete for the surface of the NPs as soon as they are introduced into the body. Initially, proteins with higher concentration in human serum would dominate the surface of the NPs, forming a protein corona (PC). These would eventually be replaced by serum proteins with significantly slower binding kinetics and higher binding affinities due to their lower concentrations [32,33].

Lysozyme (molecular weight: 14.3 kDa), a small globular protein, has a concentration of approximately 7–13 mg/L in human serum [34]. The concentration of lysozyme is maxima in human tears (1568 mg/L) [35]. It is an antibacterial enzymatic protein that is also known to reversibly interact with several endogenous and exogenous ligands [36], and has also been used for studying interactions between proteins and NPs. There are six tryptophan (Trp28, 62, 63, 108, 111, and 123) residues and four disulfide linkages within the lysozyme matrix [37]. Of the six Trp residues, Trp62 and Trp108 (located within the substrate binding site) contribute approximately 80% to the total intrinsic fluorescence of lysozyme [38]. The cleft or substrate binding site of lysozyme is surrounded by two functional domains, the α-helix and β-sheet [37,39]. Hen egg-white lysozyme (HEWL) is amongst most common model protein used for the analysis of protein-ligand/nanoparticle interactions, as it bears approximately 60% sequence similarity to that of the human lysozyme [40].

Looking at the surface properties of biocompatible AgNPs, polyphenols adsorbed at the surface of NPs may influence the degree and type of interactions with proteins. Several articles have been reported on the basis of interactions of epigallocatechin gallate (EGCG) [41] and other dietary polyphenols with carrier proteins [41–43]. However, studies concerning polyphenol-coated NPs remain elusive. Notably, the polyphenol-mediated synthesis of silver nanoparticles (AgNPs) is an area of growing interest, but an extensive literature search yielded only two results for the interaction of polyphenol-mediated synthesized AgNPs or gold nanoparticles (AuNPs) with proteins. Abraham et al. [29] reported the synthesis of AgNPs using curcumin and EGCG and their interactions with human serum albumin. Another report by Yue et al. [44] synthesized AuNPs using morin as the reducing agent and studied their interaction with bovine serum albumin. Hence, it is essential to consider the direct interactions of these biocompatible AgNPs with the carrier proteins, since during the synthesis procedure, the functional groups of the associated polyphenols might be modified. This in turn could influence the mode of binding with carrier proteins. Thus, studying the interactions of biocompatible AgNPs with HEWL is novel and would open up avenues for further research in this domain.

The focus of this study was the synthesis of AgNPs using GT extract and two of its components, EGCG and (+)-catechin (Ct) [45], and elucidated their anti-bacterial and anti-cancer activities along with their physiochemical interactions with HEWL. The reason for choosing GT and its two components is that these phytochemicals have been extensively studied for their therapeutic potential. Polyphenols such as kaempferol, EGCG, and chrysin functionalized Ag, or AuNPs have been shown to have cytotoxic effects on the MCF-7 cancer cell line [46], in treating prostate cancer [47] and in breast cancer [16], respectively. Furthermore, as stated earlier, as NPs enter the body, they come into contact with proteins; therefore, we studied the interactions of these biocompatible AgNPs with HEWL in order to identify the binding affinity and possible consequences on protein structure upon complexation.

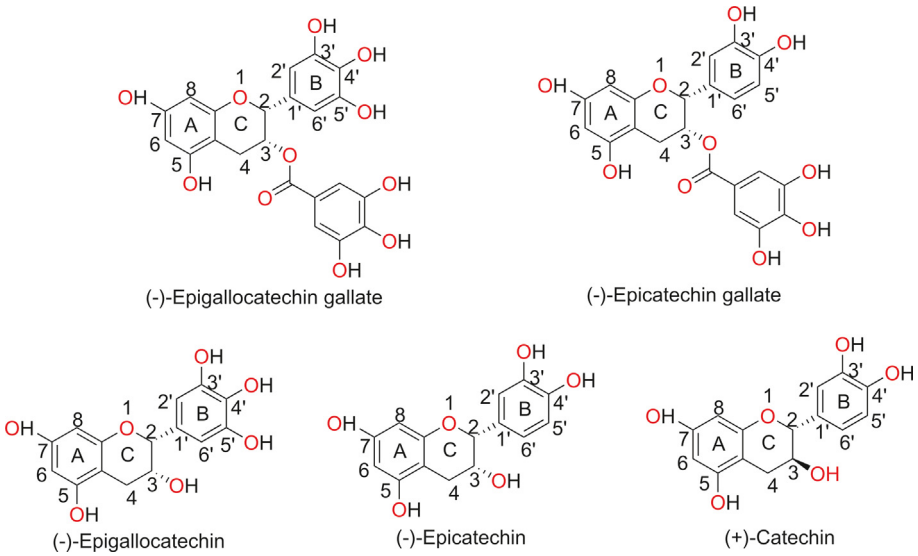

Fig. 1. Chemical structures of five primary green tea catechins [24] (Reprint from Ref. [24] with permission).

2. Materials and methods

2.1. Materials

Lipton green tea was purchased from a local grocery store in Shillong, Meghalaya, India. EGCG (E4268), Ct (C1251) and lysozyme (L6876) were procured from Sigma-Aldrich Chemical Co. (St. Louis, MO, USA). Silver nitrate (96045) and molecular biology grade Tris buffer were purchased from SRL (Mumbai, India). The stock solutions of EGCG and Ct were prepared in water and ethanol, respectively, while HEWL was prepared in Tris-HCl (20 mM, pH 7.4). HEWL concentration was measured spectrophotometrically using $\varepsilon_{280} = 37646\ M^{-1}\ cm^{-1}$. Ultrapure water was used for all experiments. Standard glassware from Borosil® (Mumbai, India) was used for the preparation of all samples. Propidium iodide (MB139), DAPI (MB097), the MTT cell assay kit (CCK003), and sterile discs (SD067) were purchased from HiMedia Laboratories (Mumbai, India). HeLa cell lines were acquired from the National Centre for Cell Science, Savitribai Phule University, Pune, India.

2.2. Methods

Detailed methodologies and experimental studies are presented in the Supplementary data. Briefly, AgNPs were synthesized at room temperature using GT extract and two of its constituent polyphenols, EGCG and Ct. Synthesized AgNPs were then characterized with the help of UV–Vis spectroscopy (PerkinElmer lambda 35 spectrometer, Singapore), Fourier-transform infrared spectroscopy (FTIR, PerkinElmer Spectrum Two, Lliantrisant, UK), Transmission electron microscopy (TEM, JEOL JEM-2100, Tokyo, Japan), Powder X-ray diffraction (P-XRD) (D8 FOCUS XRD, Karlsruhe, Germany), and the concentration of the AgNPs was determined using atomic absorption spectroscopy (AAS-ICE 3500, Loughborough, UK). Synthesized AgNPs were further screened for their antibacterial properties against bacterial strains, *Staphylococcus aureus* and *Escherichia coli*, on agar plates (Mueller-Hinton, Sisco Research Laboratories Pvt., Ltd., Mumbai, India) incubated for 18 h at 37 °C. Cytotoxic effects of the synthesized AgNPs were evaluated using the MTT assay. HeLa cells in the absence or presence of AgNPs were seeded in a 96-well plate reader, incubated for 24 h at 37 °C with 5% CO_2, and the absorbance was recorded at 595 nm using a Synergy H1 Hybrid reader, (BioTek Instrument, Winooski, VT, USA). Optical and fluorescence imaging was carried out in a Leica DMI4000 B automated inverted research microscope (Wetzlar, Germany). The fluorescence measurements were conducted on a spectrofluorometer Fluoromax-4 (Jobin Yvon, Edison, NJ, USA) using a slit width of 5/5 nm and a quartz cuvette of 1 cm path length. A JASCO J-1500 instrument (Tokyo, Japan) was used to perform the far UV-circular dichroism (CD) measurements of HEWL and its 1:1 complex with the respective AgNPs.

3. Results and discussion

3.1. Synthesis and characterization of the biocompatible AgNPs

The biocompatible AgNPs were characterized by UV–Vis absorbance spectroscopy, TEM, XRD, and FTIR studies. Absorbance spectroscopy is an excellent method for assessing the progress of biocompatible AgNPs formation by monitoring the surface plasmon resonance (SPR) band. Generally, metal NPs are known to display SPR phenomenon, in which metal NP's conducting electrons collectively oscillate in resonance with certain wavelengths upon contact with an electromagnetic field [16]. The generation of metallic AgNPs using reducing agents was initially monitored by the formation of a yellowish-brown color as shown in Fig. 2A. Excitation of the SPR band results in a color change of the aqueous solution in the UV–Vis region. The UV–Vis absorbance spectra as a function of time for the synthesized AgNPs using GT extract, EGCG, and Ct, respectively, are compared in Figs. 2B–D. Synthesized AgNPs showed SPR bands in the range of 420–430 nm, and with the progress of time the absorbance value increased which suggest the efficient formation of AgNPs. The preliminary results obtained from the absorbance studies indicated that GT extract, EGCG, and Ct can be used as effective natural reducing agents to fabricate biocompatible AgNPs without the addition of any other hazardous chemicals. The influence of temperature (5–35 °C) on the synthesis of AgNPs is also shown in Fig. S1. It could be seen that for GT extract–mediated AgNPs synthesis, no significant shift in the absorbance maxima was observed with increasing temperature, but a decrease in absorbance value was observed. Similarly, for EGCG–mediated AgNPs synthesis, the absorbance of the SPR peak decreased with increasing temperature without any noticeable shift in the peak maxima. For Ct–mediated AgNPs synthesis, a significant shift towards longer wavelength along with a decrease in the absorbance value could be observed with the rise in temperature. The effect of pH on AgNPs formation was also monitored, as shown in Fig. S2. The reaction pH can influence the electrical charges of the polyphenols, which in turn can affect their reducing/capping ability. Upon increasing the pH (6.5–9.0) of the reaction medium, a subsequent red shift was observed in the SPR peak along with an increase in the absorbance value, which can be attributed to the increase in the size of the synthesized AgNPs.

The XRD pattern of the synthesized biocompatible AgNPs using GT extract, EGCG, and Ct as reducing/capping agents is depicted in Fig. 3. The XRD peaks were observed at 38.75°, 44.85°, 64.62°, 78.01 for GT-AgNPs, 38.36°, 44.55°, 64.72°, 77.61° for EGCG-AgNPs, and 38.65°, 44.75°, 64.32°, 77.91° for Ct-AgNPs, corresponding to (111), (200), (220), and (311) planes for Bragg's reflection, respectively, for a face-centered cubic (FCC) lattice of silver (JCPDS, file no. 04–0783) [8,48]. Similar results have been reported by other research groups [12,48,49]. In addition, the reflections were sharp and had a good intensity, further illustrating the synthesized AgNPs crystalline existence [12]. The peak at the (111) plane was much more intense than that of the other planes, indicating that the (111) plane is the predominant orientation [50]. The unassigned peaks (marked as *) might be due to the presence of sample impurities or may be associated with the amorphous and crystalline organic phases [18,48].

The bioreduced AgNPs had a very small size range with a mean diameter between 10 and 30 nm, as revealed by the TEM measurements. Recent studies have reported that NPs having a diameter less than 50 nm can easily permeate into cells [51], indicating that the biocompatible AgNPs synthesized here are within an acceptable range for prospective biological applications. TEM analysis indicated that the synthesized AgNPs using GT extract (Fig. 4A) and EGCG (Fig. 5A) were non-uniform in morphology. For Ct-AgNPs (Fig. 6A), the morphology was observed to be uniform and mostly spherical in shape. GT extract and its two constituent polyphenols play a significant role in the reduction of Ag^+ ions, as stabilizing or capping agents in the synthesis of AgNPs, and may therefore have an effect on the morphology of biocompatible AgNPs. The selected area of electron diffraction pattern indicated that the AgNPs are crystalline in nature, and the bright circular rings (Figs. 4B, 5B and 6B) signify the presence of different AgNP planes that are in agreement with the results of the XRD study [8,48]. Moreover, the magnified TEM micrographs in Figs. 4C, 5C and 6C show the excellent crystalline nature of the biocompatible AgNPs [8,48]. The calculated distance of ~0.23 nm between lattice planes (Figs. 4C, 5C and 6C) corresponds to the (111) lattice spacing of FCC Ag ($d_{111} = 0.2359$ nm) [52]. Moreover, Fig. S3 shows the

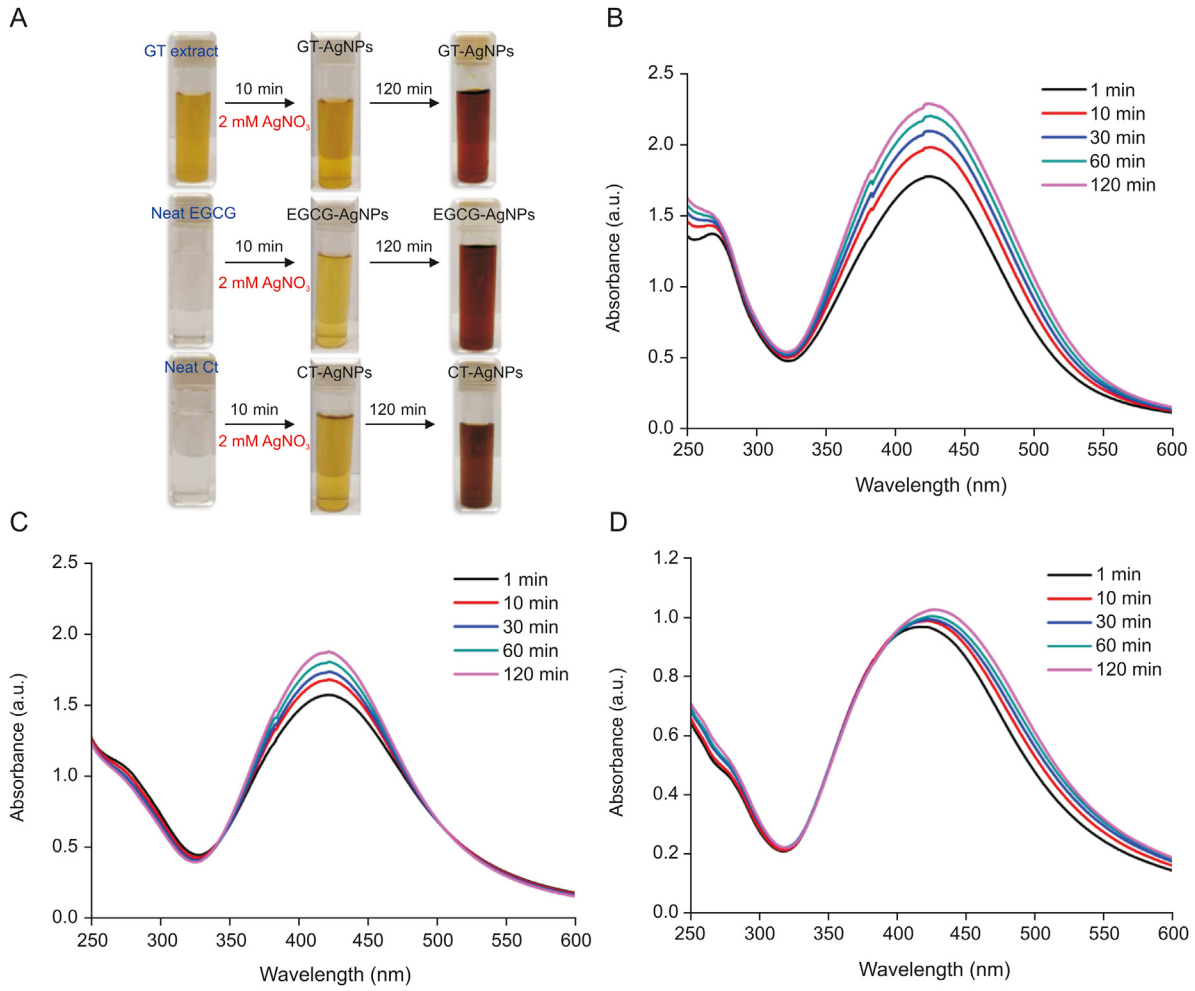

Fig. 2. (A) Development of a brown color solution with time, indicating the synthesis of silver nanoparticles (AgNPs). Time-dependent formation of AgNPs synthesized using (B) green tea (GT) extract, (C) (−)-epigallocatechin gallate (EGCG), and (D) (+)-catechin (Ct) as monitored from absorbance spectroscopy which displays an intense SPR peak at ~420 nm.

energy dispersive X-ray spectroscopy analysis of the AgNPs synthesized using GT extract, EGCG, and Ct, which serve as an excellent elemental analysis technique. Fig. S3 shows the strong elemental signal of Ag at 3.0 keV, which indicates the formation of AgNPs by the reducing agents GT extract, EGCG and Ct. The peak at approximately 8.0 keV corresponds to Cu, as the samples were drop−casted in Cu grids [27]. The presence of other elements like C and O indicates the presence of organic polyphenols in the system [53].

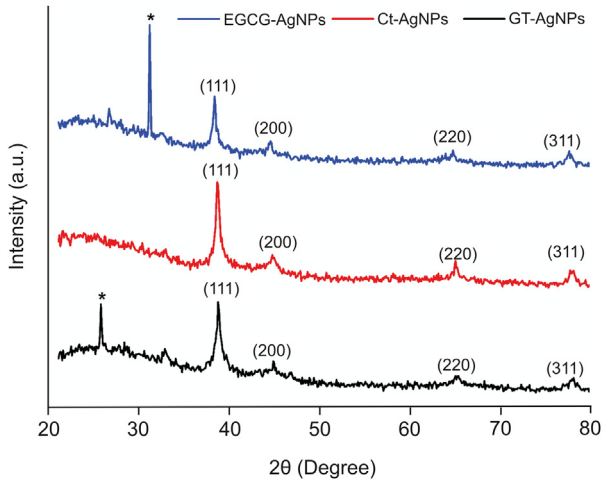

Fig. 3. Power X-ray diffraction pattern of the bio-synthesized AgNPs showing the diffraction index for face-centered cubic AgNPs.

FTIR was used to identify the possible substituents of the polyphenols that aid the formation of AgNPs (Fig. S4). In the case of GT extract synthesized AgNPs, we observed that the peaks corresponding to the native GT extract were different from the synthesized GT-AgNPs. For native EGCG, the characteristic frequency of the vibrational mode corresponding to the O−H in plane bending observed at 1344 cm^{-1} shifted to 1365 cm^{-1} upon formation of EGCG-AgNPs. In addition, the peak at 1145 cm^{-1} for the O−H aromatic vibrations shifted to 1178 cm^{-1} [29] in the NPs. The characteristic vibrations of the ester C=O group of EGCG at 1691 cm^{-1} shifted to 1701 cm^{-1} [54]. This indicates that the formation of AgNPs by EGCG probably occurs through the involvement of the −OH groups. This observation is complementary with the findings of Abraham et al. [29] where AgNPs synthesis was carried out using EGCG. In case of Ct−synthesized AgNPs, we observed that the FTIR spectrum of Ct-AgNPs was different from that of the native Ct. The frequencies of free Ct were observed to be at 1610 cm^{-1}, 1515 cm^{-1},

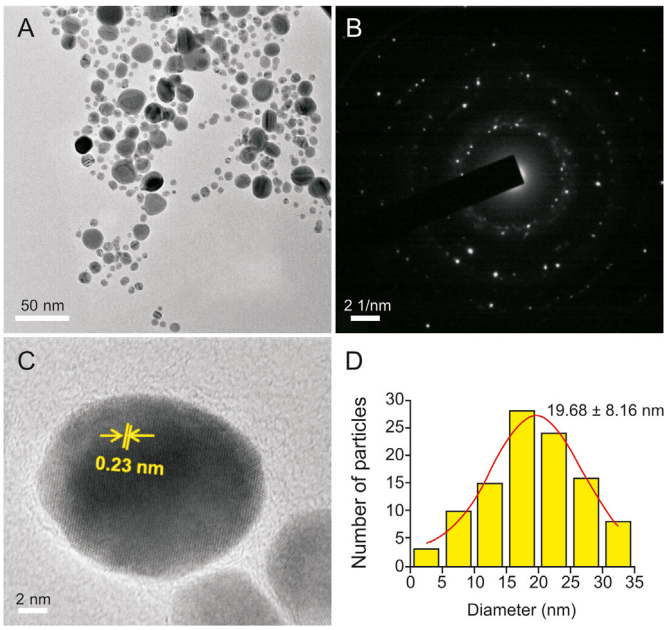

Fig. 4. (A) Transmission electron micrograph of the well-dispersed GT-AgNPs. (B) Selected area of electron diffraction pattern, and (C) a high-magnification single AgNP image showing 0.23 nm lattice fringes. (D) Particle size distribution histogram of the synthesized GT-AgNPs.

and 1474 cm^{-1} corresponding to C=C alkenes, C=C aromatic rings, and C–H alkanes, respectively [55]. The peaks at 1144 and 1281 cm^{-1} corresponding to –OH deformation of the aromatic alcohol disappeared upon formation of AgNPs [55,56]. The peak at 1023 cm^{-1} was due to the C–O stretch of the secondary alcohol and shifted to 1046 cm^{-1} [56]. These observations indicate that similar to EGCG, the –OH groups of Ct are probably involved in the reduction of Ag^{+} to AgNPs.

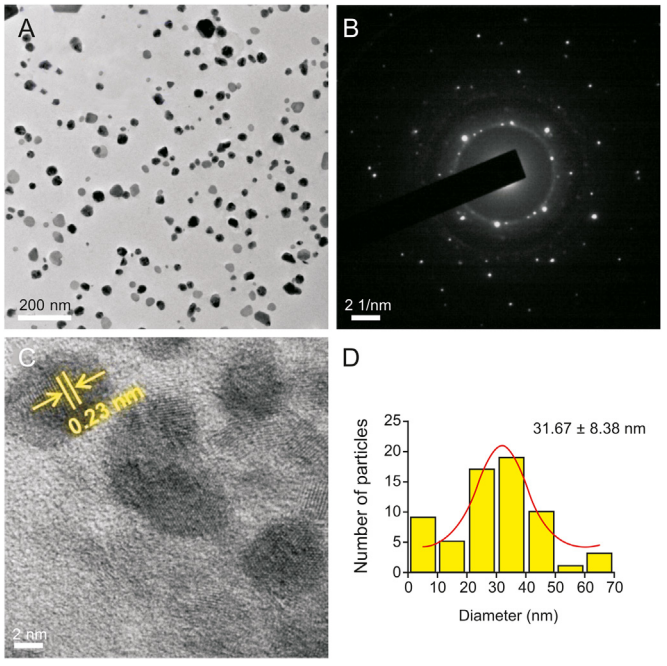

Fig. 5. (A) Transmission electron micrograph of well-dispersed EGCG-AgNPs. (B) Selected area of electron diffraction pattern, and (C) a high-magnification single AgNP image showing 0.23 nm lattice fringes. (D) Particle size distribution histogram of the synthesized EGCG-AgNPs.

3.2. Absorption studies for the binding of HEWL with AgNPs

The enhancement of absorbance of proteins at 280 nm (which arises due to the aromatic residues) upon the addition of NPs is due to the complexation of the NPs with proteins and has been used to establish the type of interaction responsible for complex formation [29,57]. Hence, the influence of the synthesized AgNPs on the absorbance profile of a fixed concentration of HEWL at 280 nm was examined. The corresponding profiles are depicted in Fig. 7. It should be noted that the 280 nm peak absorbance increased with the addition of synthesized AgNPs, and the difference spectrum of (HEWL + AgNPs)-AgNPs did not overlap with that of the native HEWL for each of the synthesized AgNPs. This indicates that complexation takes place in the ground state. Similar observations for the interactions of NPs with proteins have been previously reported [29]. The effects of the GT–, EGCG– and Ct–synthesized AgNPs on the absorption profile of HEWL were found to be similar in nature. Moreover, the effect of the binding of HEWL on the surface of the synthesized AgNPs was also monitored using the SPR band of the AgNPs at ~420 nm. In all cases, in the presence of HEWL, enhancement in the absorbance of the SPR band with a significant red shift was observed. This red shift of the SPR band is due to the adsorption of the protein on the surface (forming a PC) of the respective AgNPs. The resulting PC changes the local refractive index and also suggests that the overall hydrodynamic size of the AgNPs increases. Hence, from the absorbance measurements, it can be observed that there were strong biochemical interactions between the GT/EGCG/Ct–mediated synthesized AgNPs and HEWL. The functional groups present in proteins, such as the disulfide linkages, cysteine residues, and other thiol groups that form Ag–S linkages, also favor these interactions. The findings obtained from absorbance analysis correlate well with the literature on the conjugation of NPs with proteins [29]. Furthermore, HEWL consists of 9 negatively charged (7 aspartic acid and 2 glutamic acid) and 17 positively charged (11 arginine and 6 lysine) residues. Therefore, below its isoelectric point (~11.0) [58], HEWL possesses a net positive charge. Hence, it is likely that HEWL interacts with AgNPs

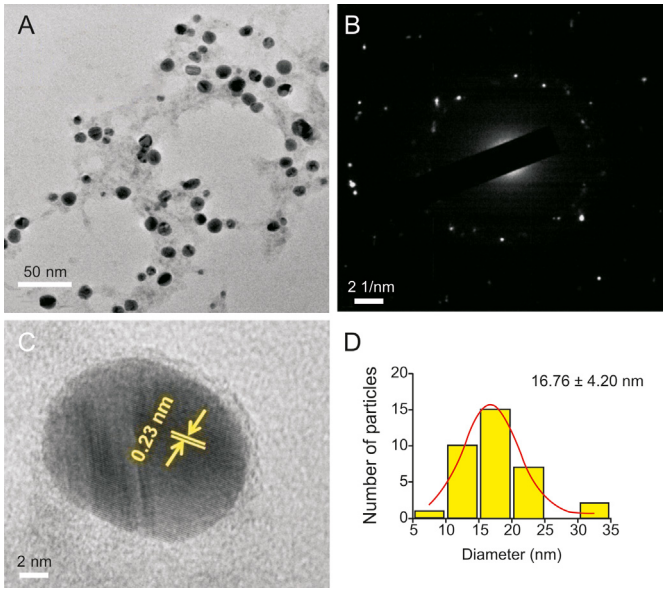

Fig. 6. (A) Transmission electron micrograph of well-dispersed Ct-AgNPs. (B) Selected area of electron diffraction pattern, and (C) a high-magnification single AgNP image showing 0.23 nm lattice fringes. (D) Particle size distribution histogram of the synthesized Ct-AgNPs.

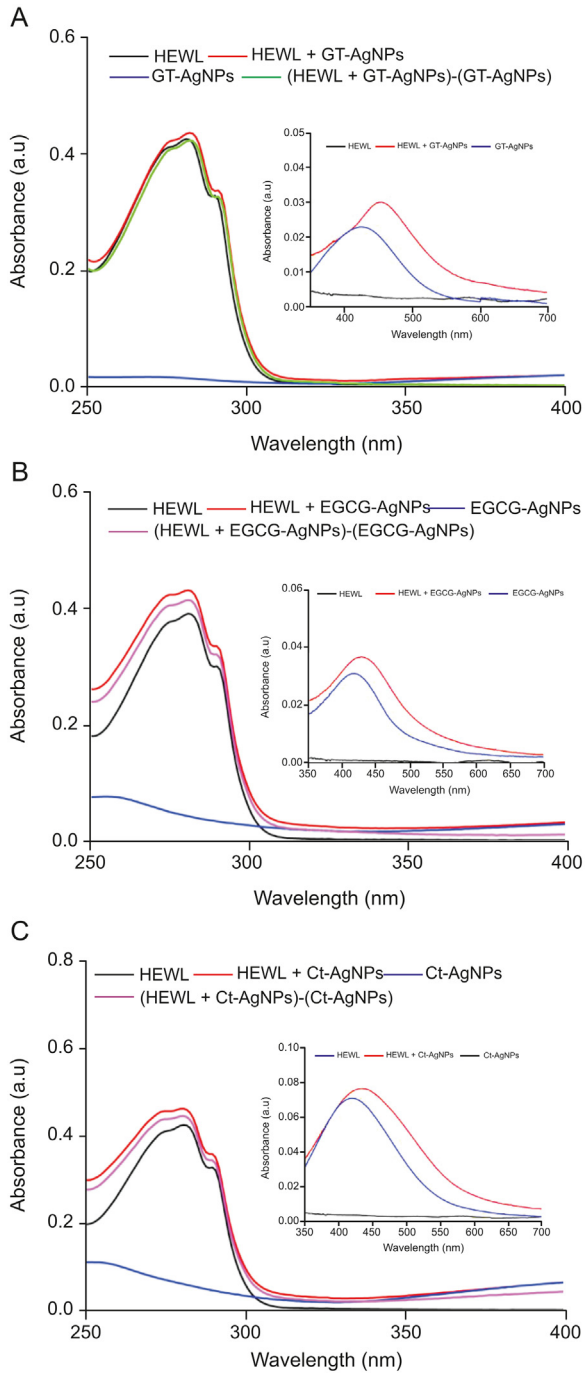

Fig. 7. The UV–Vis spectra of hen egg white lysozyme (HEWL) in the native and AgNPs bound forms, and their corresponding difference spectra for (A) GT-AgNPs (B) EGCG-AgNPs, and (C) Ct-AgNPs respectively, in the region of 250–400 nm. The inset of each figure shows the change in the surface plasmon resonance band of the respective AgNPs in the presence of HEWL. [HEWL] = [AgNPs] = 10 μM.

through electrostatic interactions, as AgNPs are generally negatively charged [29,59,60]. Several other research groups have confirmed the presence of electrostatic forces in the interaction of AgNPs with proteins [33,61,62].

3.3. Variation in the fluorescence profile of HEWL upon interaction with AgNPs

The most reliable and commonly used technique for studying protein-ligand and protein-nanoparticle interactions is fluorescence spectroscopy. In proteins, the intrinsic fluorescence originating from the Trp moieties is a vital tool for analyzing the alterations in protein structure and for making inferences about local structure and dynamics. A concentration-dependent decrease in the intrinsic fluorescence of HEWL was observed with the addition of GT-AgNPs, EGCG-AgNPs, and Ct-AgNPs. This indicates that the AgNPs affect the Trp62 and Trp108 residues. These residues are responsive to the local environment and account for ~80% of fluorescence of the protein, rendering it an important tool for binding studies. Trp62 and Trp63 of HEWL reside in the hydrophobic core, but Trp62 is relatively more exposed to the surface of the protein. It has been observed that during emission, energy transfer through the Trp108–Trp63–Trp62 sequence takes place [38]. Therefore, Trp62 may be considered as an important residue affected by AgNPs during the quenching process. In Fig. 8A, it can be observed that GT-AgNPs did not affect emission maxima of HEWL, whereas EGCG shifted the emission maxima towards a higher wavelength by 4 nm (Fig. 8B), Ct-AgNPs caused a blue shift of 2 nm (Fig. 8C). These shifts in the fluorescence emission maxima of HEWL indicate the direct influence of the AgNPs, such that the Trp residues are more exposed to the aqueous solution (hydrophilic environment) in the case of EGCG-AgNPs, and towards a more hydrophobic surrounding in Ct-AgNPs. Moreover, it was observed that the tryptophanyl fluorescence decreased the most in EGCG-AgNPs (55%) as compared to the other two AgNPs. These findings suggest that there is a strong biochemical association between AgNPs and HEWL. Even though there are numerous binding possibilities of AgNPs within the matrix of HEWL, the fluorescence study showed that the synthesized AgNPs bind near the Trp62 and Trp108 residues. This may be due to the use of capping agents for the AgNPs synthesis. Earlier crystallographic studies [63] demonstrated that Ag (I) metal binds primarily to His15 of HEWL at a distance of 2.1 Å, and also has secondary binding interactions with Arg14 and Asp87 at a distance of ~2.3 Å and 2.3 Å, respectively. However, there are no reports on the exact binding location identifying the residues involved for Ag (0) within the 3D structure of HEWL.

It is known that GT polyphenols decrease the intrinsic fluorescence of HEWL [64,65]. However, the interaction of pristine EGCG with HEWL does not alter the emission maximum. This is in contrast to the AgNPs coated with EGCG in this study, where a significant red shift has been observed. The interaction of native Ct with lysozyme has not been explored until now; hence, it is not possible to comment on the quenching behavior of Ct-AgNPs towards HEWL as compared to native Ct. However, the FTIR studies suggest that the hydroxyl groups are responsible for reducing Ag^{+} ions to AgNPs and capping of the AgNPs simultaneously. It is therefore not surprising that the interaction of HEWL with tea polyphenol–coated AgNPs will not be the same as that found in the complexation of native polyphenols with HEWL.

The fluorescence decay profiles were adjusted for the internal filter effect before continuing to determine the quenching and binding parameters [66]. The Stern-Volmer equation (Eq. 1) was then used to analyze the quenching data.

$$\frac{F_0}{F_{cor}} = 1 + K_{SV}[Q] = 1 + k_q\tau_0[Q] \quad (1)$$

where Stern–Volmer constant is denoted by K_{sv}, the bimolecular quenching constant by k_q, F_0 and F_{cor} reflect the fluorescence intensities of HEWL in the free and AgNP-bound forms, respectively. [Q] is the concentration of the quencher, and τ_0 is the average fluorescence lifetime of the Trp fluorophores of the native protein. Fig. S5 depicts the linear Stern-Volmer plot between F_0/F_{cor} at 25 °C,

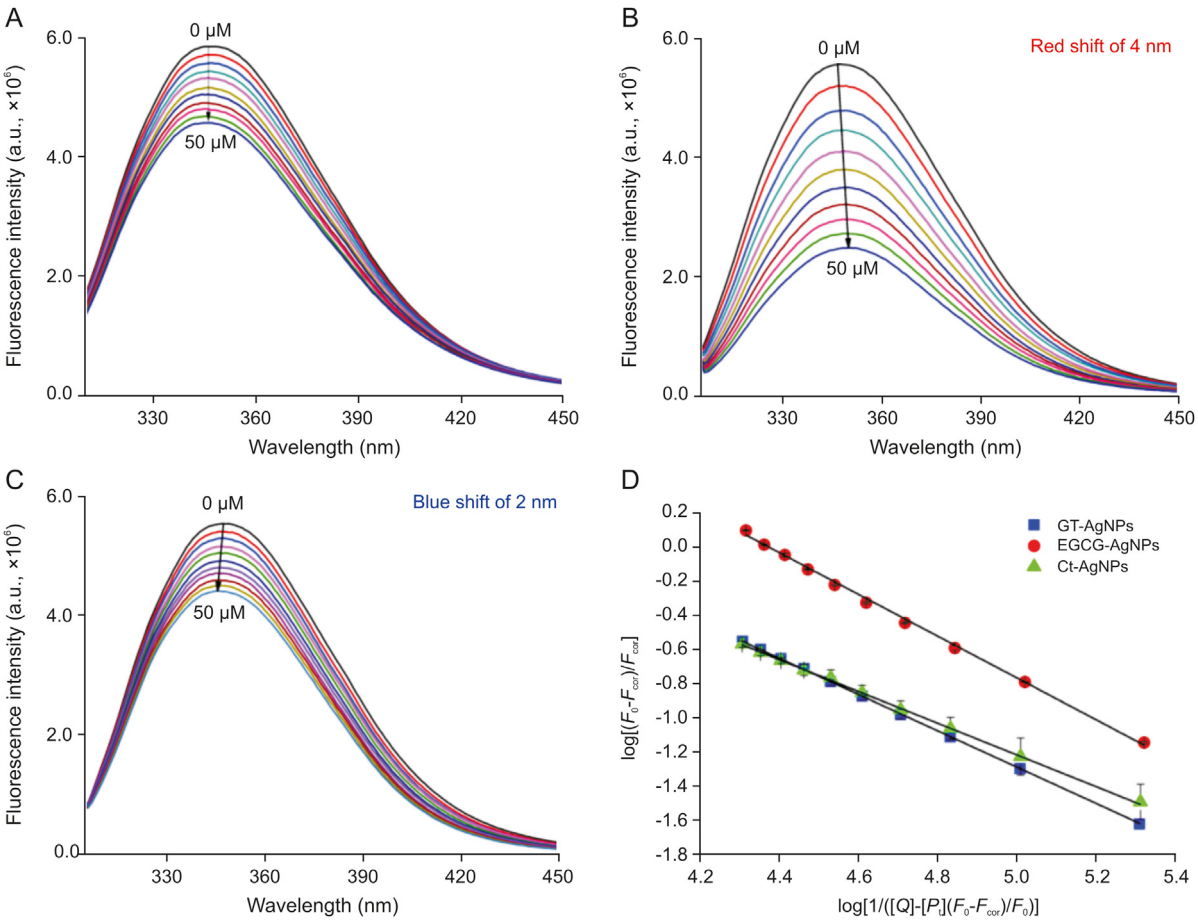

Fig. 8. Variation in the intrinsic fluorescence of 3 μM HEWL on interaction with (A) GT-AgNPs (B) EGCG-AgNPs and (C) Ct-AgNPs, and (D) represents the double log binding plots for all the three systems. λ_{ex} = 295 nm, [AgNPs] = 0–50 μM.

which indicates that the quenching is either static or dynamic in nature. The relevant parameters are listed in Table 1. The K_{sv} values of EGCG-AgNPs were higher with the order of 10^4 M^{-1}, whereas K_{sv} values of GT- and Ct-synthesized AgNPs were similar, with an order of 10^3 M^{-1}. The lifetime of HEWL in the excited state was reported to be ~1.64 ns [40]. Putting this value in Eq. (1), k_q was evaluated (Table 1). The k_q values observed were much higher than any diffusion-controlled quenching processes in water where k_q is maxima (~2×10^{10} M^{-1} s^{-1}), which suggests that the complexation of HEWL with biocompatible AgNPs takes place through a static quenching mechanism. This fact is also well supported by the absorption measurements.

The complexation of HEWL with the three biocompatible AgNPs was further assessed from the fluorescence quenching profiles. During formation of the protein-nanoparticle complexes, the proteins can have multiple associative interactions with the surface of NPs, such that the binding process may be cooperative in nature. The binding parameters were analyzed from the fluorescence profiles using the following equation (Eq. 2)

$$\log\frac{F_0 - F_{cor}}{F_{cor}} = n\log K_b - n\log\left[\frac{1}{\left([Q] - \frac{[P_t](F_0 - F_{cor})}{F_0}\right)}\right] \quad (2)$$

where $[P_t]$ and $[Q]$ are the concentrations of HEWL and AgNPs, respectively. Here, n is regarded as the Hill coefficient that reflects the degree of cooperativity of the interaction process [67,68]. For positive cooperativity, $n > 1$, which signifies that the adsorption of a protein molecule on the nanoparticle surface enhances the attachment of other protein units to the same surface. In contrast, for negative cooperativity, $n < 1$, which means that when additional proteins are adsorbed to the surface, the binding affinity of the protein gradually decreases, and $n = 1$ reflects non-cooperative interactions where the resulting binding of protein is independent of the proteins already bound to the surface [60,68]. The linear

Table 1
Binding parameters obtained for the interaction of hen egg white lysozyme (HEWL) with green tea (GT) silver nanoparticles (AgNPs), (−)-epigallocatechin gallate (EGCG)-AgNPs, and (+)-catechin (Ct)-AgNPs at 25 °C.

Complex	K_{SV} (10^4, M^{-1})	k_q (10^{13}, M^{-1} s^{-1})	K_b (10^4, M^{-1})	n	ΔG (kJ/mol)
GT-AgNPs	0.552 ± 0.035	0.336	0.621 ± 0.119	1.067 ± 0.002	−21.644 ± 0.047
EGCG-AgNPs	2.211 ± 0.016	1.348	2.309 ± 0.018	1.220 ± 0.003	−24.928 ± 0.009
Ct-AgNPs	0.548 ± 0.035	0.334	0.479 ± 0.057	1.042 ± 0.101	−20.985 ± 0.300

double log plot of $\log[(F_0 - F_{cor})/F_{cor}]$ against $\log[1/([Q] - [P_t](F_0 - F_{cor})/F_0)]$ for the binding of the three biocompatible AgNPs is shown in Fig. 8D and the parameters obtained are listed in Table 1. According to the values of n for binding, EGCG-AgNPs showed greater cooperativity than the other NPs (Table 1), indicative of a positive cooperativity in binding. These observations clearly suggest that when a molecule of HEWL is adsorbed on the surface of the AgNPs, the binding of other HEWL units increases, leading to the formation of a dense PC around the surface of the AgNPs. As shown in Table 1, EGCG-AgNPs had the highest binding affinity towards HEWL, with a binding constant (K_b) value of $(2.309 \pm 0.018) \times 10^4$ M^{-1} followed by GT-AgNPs and then Ct-AgNPs (binding order of 10^3 M^{-1}). The spontaneity of the association of the AgNPs with HEWL was evaluated using Gibb's equation (Eq. (3)), and the negative ΔG values for the complexation of the three AgNPs with HEWL individually indicate the spontaneity of the interaction process.

$$\Delta G = -2.303\, RT \log K_b \quad (3)$$

3.4. Fluorescence resonance energy transfer (FRET) study: distance between the fluorophore and the AgNPs

Interactions between protein–ligand and nanoparticle can lead to the transfer of energy from a fluorophore (donor) of the protein via non-radiative pathways to acceptor ligand/nanoparticle. The energy transfer from the two dominant fluorophores of HEWL (Trp62 and Trp108) to the biocompatible AgNPs could therefore be assessed with the aid of the FRET principle of Förster theory. A significant overlap between the donor fluorescence molecule and the acceptor absorption is one of the prerequisites for FRET. According to Imoto et al. [38], the fluorescence of HEWL emanates from the Trp62 and Trp108 residues, and the fluorescence quenching studies discussed above prove that the three biocompatible AgNPs mainly quench the fluorescence arising from these residues. Fig. S6 shows the spectral overlap between the fluorescence of HEWL and the absorbance profiles of the respective AgNPs. The efficiency of energy transfer (E), the overlap integral $J(\lambda)$, critical distance at 50% energy transfer (R_0), and binding distance (r) for the interactions of HEWL with these biocompatible AgNPs were evaluated using Förster's theory as described by Lakowicz [66]. For the estimation of the above parameters, literature values of κ^2, Q_D, and N, corresponding to 2/3, 0.118 and 1.336, respectively, were used [40], and the estimated parameters are presented in Table 2. The distance between the donor and acceptor was less than 7 nm, indicating the possibility of FRET from HEWL to the AgNPs.

3.5. Synchronous fluorescence spectroscopy

Since its invention by Lloyd [69], synchronous fluorescence spectroscopy has been widely employed to understand the modulation within the microenvironment of protein fluorophores upon contact with ligands/NPs [69,70]. This method was basically developed to differentiate between a set of mixtures whose individual fluorescence overlaps with each other [69]. As per Miller's theory [71], fixing the wavelength interval ($\Delta\lambda$) to 60 nm and 15 nm would yield details about the Trp and Tyr moieties in the protein, respectively. Therefore, Trp/Tyr fluorescence quenching along with a shift in the emission maximum by a ligand or NPs indicates the existence of specific interactions that alter the surrounding polarity of these residues. The effects of GT-AgNPs, EGCG-AgNPs, and Ct-AgNPs on synchronous fluorescence spectra of HEWL at $\Delta\lambda = 60$ nm are depicted in Fig. 9, and at $\Delta\lambda = 15$ nm in Fig. S7, respectively. It was observed that on addition of GT-AgNPs, the intensity of Trp/Tyr fluorescence decreased systematically without any shift in emission maxima indicating that GT-AgNPs have a nominal effect on the microenvironment of the Trp or Tyr residues. The incremental addition of EGCG-AgNPs reduced Trp/Tyr fluorescence, resulting in a significant red shift (5 nm) at $\Delta\lambda = 60$ nm, which suggests the enhancement of polarity around the Trp residues. At the same time, a negligible impact on the emission maxima at $\Delta\lambda = 15$ nm was observed, suggesting that EGCG-AgNPs had no impact on the microenvironment of Tyr moieties. In contrast, for Ct-AgNPs, a concentration-dependent reduction in the fluorescence of Trp and Tyr residues was observed with a blue shift (2 nm) of the emission maxima at $\Delta\lambda = 60$ nm and no observable shift at $\Delta\lambda = 15$ nm. The blue shift probably indicates that the Trp residues experience a lesser degree of exposure to the aqueous buffer and move toward a more hydrophobic environment. Such observations corroborate with those discussed in Section 3.3.

Table 2
Energy transfer parameters for the interactions between the biocompatible silver nanoparticles (AgNPs) and HEWL.

Complex	E	$J(\lambda) \times 10^{-14}$ ($M^{-1}cm^3$)	R_0 (nm)	r (nm)
HEWL + GT-AgNPs	0.014	0.198	1.870	3.782
HEWL + EGCG-AgNPs	0.085	0.599	2.248	3.353
HEWL + Ct-AgNPs	0.014	0.135	1.756	3.551

3.6. Influence of biocompatible AgNPs on the structure of HEWL

CD is an accomplished spectroscopic method that enables rapid identification of the structural composition of globular biomacromolecules in various environments, like the binding of ligands and NPs. The far–UV region (190–240 nm) is typically used to quantify the secondary structural components of proteins. Native HEWL is characterized by two negative ellipticity minima corresponding to the α-helical components, which are centered at 208 nm and 222 nm, respectively [72]. The effects of the biocompatible AgNPs synthesized using GT extract, EGCG and Ct on the secondary structure of HEWL were determined using the online server DICHROWEB [73], and the results are summarized in Table 3. As shown in Fig. 10, the addition of biocompatible AgNPs had no significant effect on the secondary structure of HEWL upon interaction, but it was observed that the α-helical content of the protein increased slightly from 38.90% to ~41%, whereas the β-sheet content decreased slightly. Hence, it can be concluded that binding of biocompatible AgNPs to HEWL results in a very minute alteration in the secondary structural conformation of HEWL. Similar findings were reported for the interactions of Ag, Au, and Fe NPs with HEWL [74–76].

3.7. Anti-bacterial activity of the biocompatible AgNPs

The nanodimension of AgNPs means that they have a higher surface-to-volume ratio relative to their bulk counterparts. This property of AgNPs facilitates their interaction with bacterial surfaces, which enhances the anti-bacterial propensity of AgNPs. The mechanism of action of the AgNPs towards bacterial strains, as described by Rai et al. [77], includes the attachment and penetration of the AgNPs into the bacteria. AgNPs interact with proteins (which contain sulphur) in the bacterial cell wall and DNA (which contain phosphorous) inside the cell. AgNPs affect the respiratory chain and cell division process, crippling enzymes and preventing oxygen uptake. This effectively suffocates the bacteria and eventually leads to cell death. Several other groups have reported the

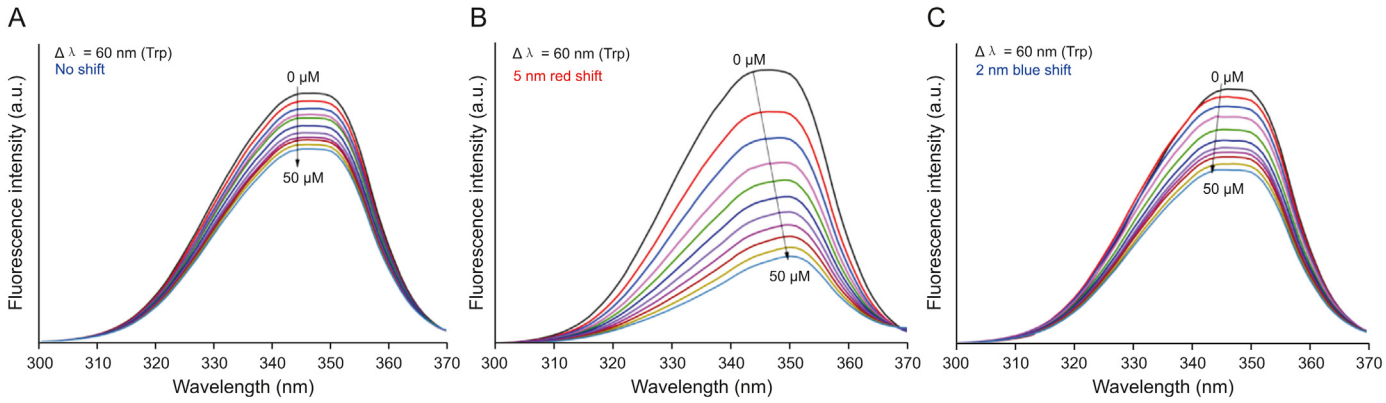

Fig. 9. Synchronous fluorescence spectra of HEWL at Δλ = 60 nm (Trp) for the interactions of (A) GT-AgNPs (B) EGCG-AgNPs and (C) Ct-AgNPs.

Table 3
Changes in the secondary elements (in %) of HEWL obtained from far UV-circular dichroism analysis.

Complex	α-helix	β-sheet	Turns	Coil
HEWL	38.90 ± 3.00	16.55 ± 3.45	20.10 ± 0.10	25.90 ± 1.70
HEWL + GT-AgNPs	40.85 ± 0.65	13.30 ± 0.30	21.65 ± 0.55	25.95 ± 0.35
HEWL + EGCG-AgNPs	41.90 ± 1.40	14.05 ± 1.45	20.00 ± 2.10	26.15 ± 0.15
HEWL + Ct-AgNPs	41.05 ± 1.25	13.55 ± 1.75	21.90 ± 1.60	25.80 ± 1.00

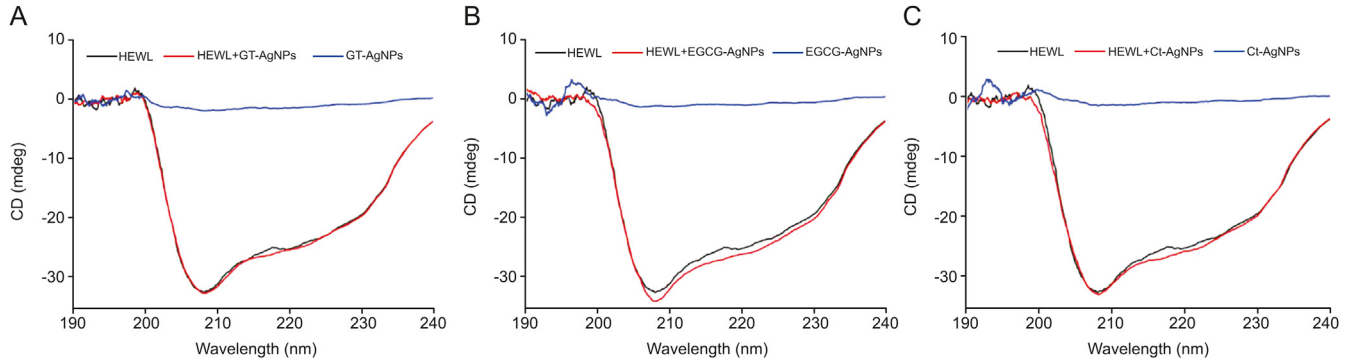

Fig. 10. Influences of AgNPs synthesized using (A) GT extract, (B) EGCG, and (C) Ct on the far UV-circular dichroism spectra of HEWL. [HEWL] = [AgNPs] = 20 μM.

antibacterial activity of the synthesized AgNPs using GT extract [78,79], but the effect of GT constituents EGCG and Ct synthesized AgNPs on the bacterial strains has not been evaluated until now. The disk diffusion method was employed to study the antibacterial effect of the three AgNPs against gram-negative (*E. coli*) and gram-positive (*S. aureus*) bacterial strains by monitoring the zone of inhibition. From Table 4 and Fig. 11, it can be seen that GT-AgNPs, EGCG-AgNPs and Ct-AgNPs showed enhanced anti-bacterial effects (growth inhibition is confirmed by the clear inhibitory zones) against both *S. aureus* and *E. coli* as compared with blank samples (free GT extract, EGCG, and Ct). It could be observed that the growth of *E. coli* was inhibited more than *S. aureus* by these biocompatible AgNPs. This enhanced bactericidal effect of AgNPs is due to the release of Ag^{+} ions from the AgNPs to bacterial cells [77,80]. These results advocate that the AgNPs synthesized using GT extract and its two active components, EGCG and Ct, are promising antibacterial agents against gram-positive and gram-negative bacteria. Moreover, the cell walls of the bacteria are strongly protected from foreign species penetration by the thick lipopolysaccharide and peptidoglycan layer. Hence, the observed antibacterial behavior of the AgNPs tested could therefore be due to the small size of the particles (20–30 nm) [81], which can permeate and pass through the nanosized cell wall pores, thus enhancing the antibacterial activity against bacterial infections. The effects of ethanol, buffer, and $AgNO_3$ on the strains of *E. coli* and *S. aureus* are shown in Fig. S8.

Table 4
Zone of inhibition of the bacterial strains in the presence of the respective AgNPs (50 μg/mL). All tests were performed in triplicates.

Compound	*E. coli* (mm)	*S. aureus* (mm)
GT-AgNPs	28.5	20.5
EGCG-AgNPs	26.5	19.0
Ct-AgNPs	28.0	21.0
Native GT extract	–	–
Native EGCG	–	–
Native Ct	–	–
$AgNO_3$	1.0	–

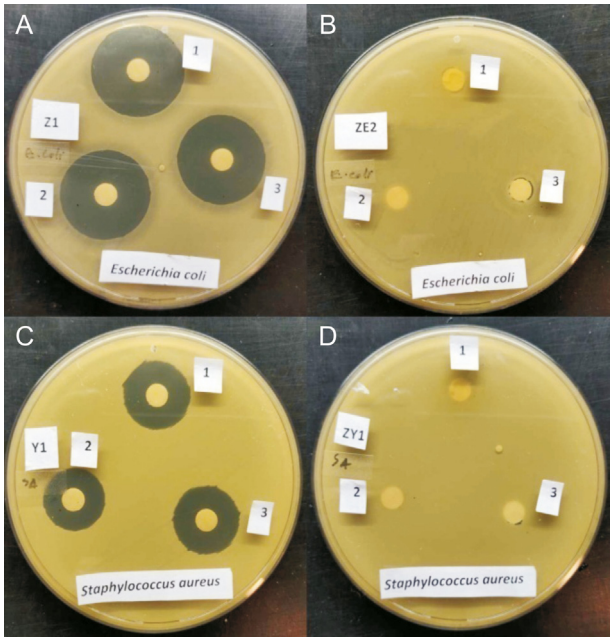

Fig. 11. Anti-bacterial efficacy of GT-AgNPs (1), EGCG-AgNPs (2), and Ct-AgNPs (3) on (A) *Escherichia coli* (*E. coli*) and (C) *Staphylococcus aureus* (*S. aureus*) bacterial strains, respectively. (B) and (D) represent the effect of pristine GT extract (1), EGCG (2), and Ct (3) on *E. coli and S. aureus* bacterial strains, respectively. The concentrations of the AgNPs and pristine capping agents were 50 μg/mL.

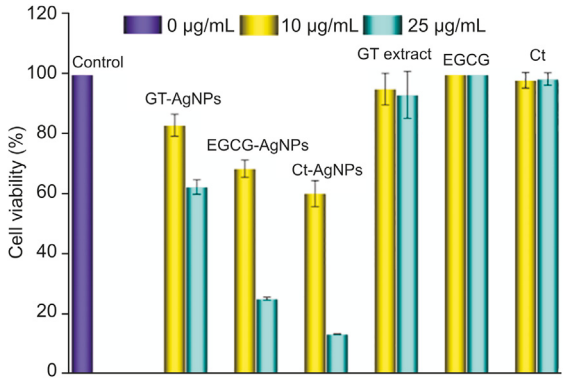

Fig. 12. In vitro MTT assay-based determination of percentage HeLa cell viability on treatment with varying concentrations (0, 10, and 25 μg/mL) of the synthesized AgNPs along with their corresponding capping/stabilizing agents.

3.8. Cytotoxic activity using MTT assay

The cytotoxic effects of the synthesized biocompatible AgNPs using GT extract, EGCG and Ct, against HeLa cell lines were studied. The percentage cell viability of the synthesized AgNPs at two different concentrations (10 μg/mL and 25 μg/mL) was compared with their respective free reducing/capping agents for a period of 24 h. Fig. 12 indicates that HeLa cell inhibition steadily increased with the concentration of AgNPs, while the free reducing/capping agents exhibited no observable cytotoxic effects at the studied concentrations. These results indicate that the cytotoxic effect of the formulated AgNPs was much stronger than that of the free reducing/capping agents. Toxicity and biokinetics depend on the factors like the shape, size, surface area, and surface functionalization of the AgNPs. The enhanced cytotoxic effect of the

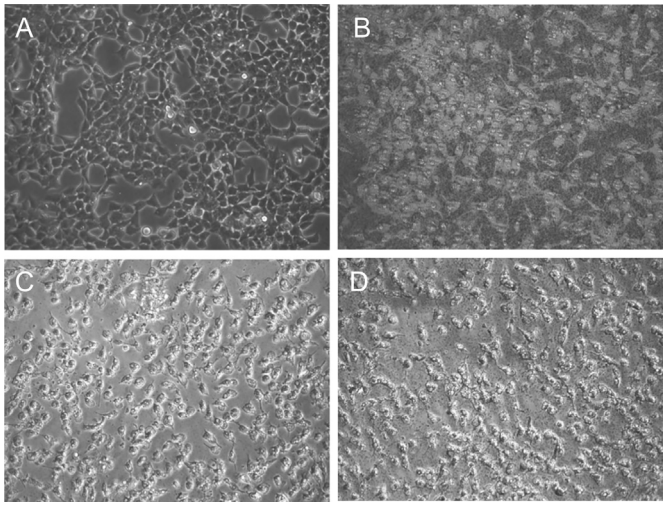

Fig. 13. Optical microscope images of (A) control (untreated) HeLa cells, (B) GT-AgNPs, (C) EGCG-AgNPs and (D) Ct-AgNPs treated HeLa cells at a concentration of 25 μg/mL. The images, including the control, were captured after 24 h of incubation.

synthesized AgNPs can be seen in the optical microscope images shown in Fig. 13. As compared to the normal or untreated HeLa cells of the control (Fig. 13A), the synthesized biocompatible AgNPs treated HeLa cells (Figs. 13B–D) showed substantial morphological changes or cell death due to cytoplasmic condensation, cell shrinkage, membrane integrity loss and inhibition of cell growth [82]. The cytotoxic effects may be due to the accumulation of AgNPs inside the cells, resulting in chemical interaction of the AgNPs within the bioenvironment of the HeLa cells, leading to enhanced stress and ultimately to cell death. Briefly, the biocompatible AgNPs may affect the phosphorus-containing DNA, which hinders the replication mechanism, resulting in the inhibition of enzyme functions. This eventually contributes to the loss of cell viability and, via apoptosis, to cell death.

Based on the observed apoptotic cell death in Fig. 13, the dual fluorescence staining method was used to further visualize cell death upon treatment with AgNPs. The fluorescence imaging analysis depends on the use of different types of fluorescent dyes; here, we chose DAPI and PI as the staining agents. DAPI is a blue fluorescent nuclear counterstain dye that binds to the minor groove (A-T sites) of ds-DNA and can penetrate through the intact cell membrane of both live (although it passes less efficiently through living cell membranes) and dead cells. PI is a red fluorescent dye that intercalates into ds-DNA and is impermeable to live cells and only binds to dead cells. Therefore, the dual DAPI/PI staining method used in AgNPs treated HeLa cells can qualitatively distinguish the influence of AgNPs. Fig. 14A illustrates the influence of DAPI/PI dyes on untreated HeLa cells, it can be observed that most of the cells were alive and the number of dead cells was minimal (PI treated). Figs. 14B–D shows that upon treatment with the respective AgNPs (25 μg/mL), i.e., GT-AgNPs, EGCG-AgNPs, and Ct-AgNPs, the number of dead cells increased (PI treated). Thus, the synthesized AgNPs resulted in apoptosis of HeLa cells. This indicates that a significant number of AgNPs could assemble inside HeLa cells, resulting in an increased stress, and finally leading to cell death. These findings clearly highlight the increased efficacy of GT–, EGCG–, and Ct–functionalized AgNPs against HeLa cells.

3.9. Mechanism of AgNPs synthesis using polyphenols of GT

The mechanism of AgNP or any other NP formation mediated by polyphenols has not been fully understood to date. Hence, we

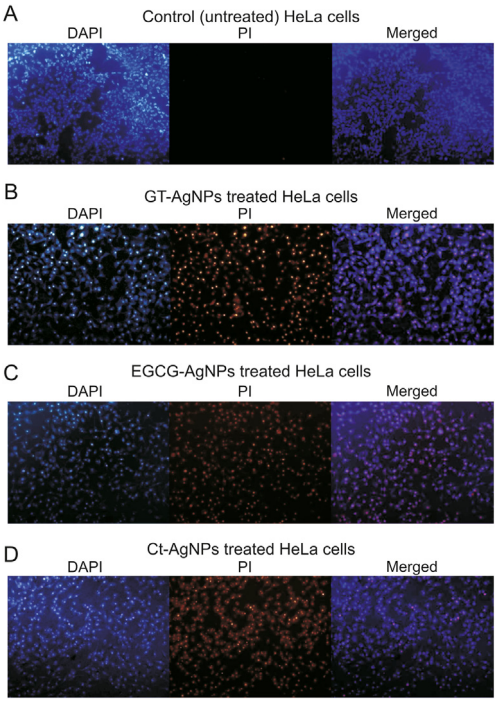

Fig. 14. Fluorescence imaging using the dual staining method on untreated and AgNPs treated HeLa cells.

would recommend caution in making generalized predictions regarding the mechanism responsible in the formation of AgNPs using polyphenols. It is known that in addition to the reduction of Ag^{+} to Ag^{0}, polyphenols grant stability to NPs by functioning as capping agents. GT is composed of several polyphenols as shown in Fig. 1. These polyphenols, as the name suggests, consist of more than one −OH group in their skeleton, which, according to several groups, are the main reducing agents responsible for AgNP synthesis [18,83]. According to Jain and Mehata [18] the tautomeric enol to keto transformation of polyphenols may release a reactive hydrogen atom that helps with the reduction of Ag^{+} to AgNPs. Raghavan et al. [46] demonstrated the role of −OH groups attached to the catechol ring of kaempferol in the synthesis of AuNPs. Therefore, based on the FTIR studies, we believe that the hydroxyl moieties of the polyphenols are responsible for the synthesis of the respective AgNPs.

4. Conclusion

The use of plant extracts to synthesize metal NPs is not limited; however, synthesis of NPs using pure polyphenols is meager. Therefore, here we report the use of GT extract and two of its constituent polyphenols to synthesize AgNPs. The antioxidant capability of GT polyphenols shows a significant potential as 'soft' capping/reducing agents for nanoparticle synthesis. The synthesized AgNPs showed an intense absorption SPR peak, and were found to be crystalline in nature with a lattice spacing of 0.23 nm. Polyphenolic −OH groups were responsible for reducing Ag^{+} to AgNPs. The synthesized AgNPs showed remarkable anti-bacterial effects against *E. coli* and *S. aureus* bacterial strains and enhanced cytotoxic effects against HeLa cells. When NPs are introduced into the body, a PC formation on the surface of the metal NPs occurs; therefore, we studied the binding affinity of these synthesized AgNPs towards HEWL. The AgNPs quenched the intrinsic fluorescence of HEWL via the static quenching mode. The binding constant of the three AgNPs towards HEWL was found to decrease in the following order EGCG-AgNPs > GT-AgNPs > Ct-AgNPs. Moreover, EGCG-AgNPs increased the polarity around the Trp fluorophore, whereas Ct-AgNPs had the opposite effect, and GT-AgNPs had no observable impact. This suggests that the surface capping of the respective AgNPs affects the shift in polarity in the vicinity of Trp fluorophore. The AgNPs did not cause a major change in the secondary structure of HEWL. The current study focused on the synthesis of biocompatible AgNPs and understanding their antibacterial, cytotoxic and protein-nanoparticle interactions, suggesting the potential benefits of the polyphenols. The result obtained appears promising, but as most of the experiments were carried out under in vitro conditions, it would require further in vivo studies to corroborate the results. For example, the behavior of AgNPs should be studied in the presence of blood plasma, which will offer a more detailed understanding of the protein-nanoparticle complexation. In general, the use of such bio-active natural polyphenols with −OH functional groups to synthesize metal NPs would create new opportunities in the fields of nanomedicine and nanodiagnostics.

Declaration of competing interest

The authors declare that there are no conflicts of interest.

Acknowledgments

Atanu Singha Roy acknowledges the Science and Engineering Research Board (ECR File No. ECR/2016/000159 and CRG File No. CRG/2019/000852), Government of India, for funding this work. The authors thank the Department of Bioscience and Bioengineering, IIT Guwahati for CD measurements. Sourav Das is indebted to TEQIP-III NIT Meghalaya and MH thanks NIT Meghalaya for fellowship. The authors acknowledge Sophisticated Analytical Instrumentation Centre, Tezpur University for P-XRD and Sophisticated Analytical Instrument Facility, North Eastern Hill University (Shillong) for the TEM and energy dispersive X-ray spectroscopy measurements, respectively. Sourav Das would like to thank Amanda N. Abraham, School of Science, RMIT University, Australia, for guidance on the determination of AgNP concentration in the colloidal phase using atomic absorption spectrometry.

Appendix A. Supplementary data

Supplementary data to this article can be found online at https://doi.org/10.1016/j.jpha.2020.12.003.

References

[1] L.A. Dykman, N.G. Khlebtsov, Gold nanoparticles in biology and medicine: recent advances and prospects, Acta Naturae 3 (2011) 34–55.
[2] P. Di Pietro, G. Strano, L. Zuccarello, et al., Gold and silver nanoparticles for applications in theranostics, Curr. Top. Med. Chem. 16 (2016) 3069–3102.
[3] H. Chugh, D. Sood, I. Chandra, et al., Role of gold and silver nanoparticles in cancer nano-medicine, Artif. Cells, Nanomed. Biotechnol. 46 (2018) 1210–1220.
[4] Z. Sadowski, in: Biosynthesis and Application of Silver and Gold Nanoparticles, Silver Nanoparticles, IntechOpen, Rijeka, 2012, pp. 258–276.
[5] A. Kumar, P.K. Vemula, P.M. Ajayan, et al., Silver-nanoparticle-embedded antimicrobial paints based on vegetable oil, Nat. Mater. 7 (2008) 236–241.
[6] S. Gurunathan, K. Kalishwaralal, R. Vaidyanathan, et al., Biosynthesis, purification and characterization of silver nanoparticles using Escherichia coli, Colloids Surf. B Biointerfaces 74 (2009) 328–335.
[7] X.-F. Zhang, Z.-G. Liu, W. Shen, et al., Silver nanoparticles: synthesis, characterization, properties, applications, and therapeutic approaches, Int. J. Mol. Sci. 17 (2016), 1534.
[8] M.N. Nadagouda, N. Iyanna, J. Lalley, et al., Synthesis of silver and gold nanoparticles using antioxidants from blackberry, blueberry, pomegranate, and turmeric extracts, ACS Sustain. Chem. Eng. 2 (2014) 1717–1723.
[9] P. Pourali, S.H. Badiee, S. Manafi, et al., Biosynthesis of gold nanoparticles by

two bacterial and fungal strains, Bacillus cereus and Fusarium oxysporum, and assessment and comparison of their nanotoxicity in vitro by direct and indirect assays, Electron. J. Biotechnol. 29 (2017) 86–93.
[10] Z. Molnár, V. Bódai, G. Szakacs, et al., Green synthesis of gold nanoparticles by thermophilic filamentous fungi, Sci. Rep. 8 (2018), 3943.
[11] A. Mourato, M. Gadanho, A.R. Lino, et al., Biosynthesis of crystalline silver and gold nanoparticles by extremophilic yeasts, Bioinorgan. Chem. Appl. 2011 (2011), 546074.
[12] T. Kathiraven, A. Sundaramanickam, N. Shanmugam, et al., Green synthesis of silver nanoparticles using marine algae Caulerpa racemosa and their antibacterial activity against some human pathogens, Appl. Nanosci. 5 (2015) 499–504.
[13] J. Fei, J. Zhao, C. Du, et al., One-pot ultrafast self-assembly of autofluorescent polyphenol-based core@shell nanostructures and their selective antibacterial applications, ACS Nano 8 (2014) 8529–8536.
[14] X. Yan, J. Blacklock, J. Li, et al., One-pot synthesis of polypeptide-gold nanoconjugates for in vitro gene transfection, ACS Nano 6 (2012) 111–117.
[15] C. Manach, A. Scalbert, C. Morand, et al., Polyphenols: food sources and bioavailability, Am. J. Clin. Nutr. 79 (2004) 727–747.
[16] G. Sathishkumar, R. Bharti, P.K. Jha, et al., Dietary flavone chrysin (5,7-dihydroxyflavone ChR) functionalized highly-stable metal nanoformulations for improved anticancer applications, RSC Adv. 5 (2015) 89869–89878.
[17] N. Sahu, D. Soni, B. Chandrashekhar, et al., Synthesis of silver nanoparticles using flavonoids: hesperidin, naringin and diosmin, and their antibacterial effects and cytotoxicity, Int. Nano Lett. 6 (2016) 173–181.
[18] S. Jain, M.S. Mehata, Medicinal plant leaf extract and pure flavonoid mediated green synthesis of silver nanoparticles and their enhanced antibacterial property, Sci. Rep. 7 (2017), 15867.
[19] Y. Miyata, T. Matsuo, K. Araki, et al., Anticancer effects of green tea and the underlying molecular mechanisms in bladder cancer, Medicines 5 (2018), 87.
[20] Z.D. Ozdal, E. Sahmetlioglu, I. Narin, et al., Synthesis of gold and silver nanoparticles using flavonoid quercetin and their effects on lipopolysaccharide induced inflammatory response in microglial cells, 3 Biotech 9 (2019), 212.
[21] S. Kakutani, H. Watanabe, N. Murayama, Green tea intake and risks for dementia, Alzheimer's disease, mild cognitive impairment, and cognitive impairment: a systematic review, Nutrients 11 (2019), 1165.
[22] Green tea consumption, World Green Tea Association, http://www.o-cha.net/english/teacha/distribution/greentea3.html. (accessed on 5 November, 2019).
[23] W.C. Reygaert, An update on the health benefits of green tea, Beverages 3 (2017), 6.
[24] N. Miyoshi, M. Pervin, T. Suzuki, et al., Green tea catechins for well-being and therapy: prospects and opportunities, Botanics Targets Ther. 5 (2015) 85–96.
[25] V. Sanna, N. Pala, G. Dessì, et al., Single-step green synthesis and characterization of gold-conjugated polyphenol nanoparticles with antioxidant and biological activities, Int. J. Nanomed. 9 (2014) 4935–4951.
[26] L.A. Levchenko, S.A. Golovanova, N.V. Lariontseva, et al., Synthesis and study of gold nanoparticles stabilized by bioflavonoids, Russ. Chem. Bull. 60 (2011), 426.
[27] F.J. Osonga, A. Akgul, I. Yazgan, et al., Flavonoid-derived anisotropic silver nanoparticles inhibit growth and change the expression of virulence genes in Escherichia coli SM10, RSC Adv. 8 (2018) 4649–4661.
[28] M.C. Moulton, L.K. Braydich-Stolle, M.N. Nadagouda, et al., Synthesis, characterization and biocompatibility of "green" synthesized silver nanoparticles using tea polyphenols, Nanoscale 2 (2010) 763–770.
[29] A.N. Abraham, T.K. Sharma, V. Bansal, et al., Phytochemicals as dynamic surface ligands to control nanoparticle-protein interactions, ACS Omega 3 (2018) 2220–2229.
[30] M. Mahmoudi, M.A. Sahraian, M.A. Shokrgozar, et al., Superparamagnetic iron oxide nanoparticles: promises for diagnosis and treatment of multiple sclerosis, ACS Chem. Neurosci. 2 (2011) 118–140.
[31] A.A. Shemetov, I. Nabiev, A. Sukhanova, Molecular interaction of proteins and peptides with nanoparticles, ACS Nano 6 (2012) 4585–4602.
[32] T. Cedervall, I. Lynch, S. Lindman, et al., Understanding the nanoparticle-protein corona using methods to quantify exchange rates and affinities of proteins for nanoparticles, Proc. Natl. Acad. Sci. Unit. States Am. 104 (2007) 2050–2055.
[33] P.S. Nayak, S.M. Borah, H. Gogoi, et al., Lactoferrin adsorption onto silver nanoparticle interface: implications of corona on protein conformation, nanoparticle cytotoxicity and the formulation adjuvanticity, Chem. Eng. J. 361 (2019) 470–484.
[34] J. Hankiewicz, E. Swierczek, Lysozyme in human body fluids, Clin. Chim. Acta 57 (1974) 205–209.
[35] E. Aine, P. Mörsky, Lysozyme concentration in tears-assessment of reference values in normal subjects, Acta Ophthalmol. 62 (1984) 932–938.
[36] S. Das, S. Santra, M.A. Rohman, et al., An insight into the binding of 6-hydroxyflavone with hen egg white lysozyme: a combined approach of multi-spectroscopic and computational studies, J. Biomol. Struct. Dyn. 37 (2019) 4019–4034.
[37] C.C.F. Blake, D.F. Koenig, G.A. Mair, et al., Structure of hen egg-white lysozyme, a three dimensional fourier synthesis at 2-Ångstroms resolution, Nature 206 (1965) 757–761.
[38] T. Imoto, L.S. Forster, J.A. Rupley, et al., Fluorescence of lysozyme: emissions from tryptophan residues 62 and 108 and energy migration, Proc. Natl. Acad. Sci. U. S. A. 69 (1972) 1151–1155.
[39] L.J. Smith, M.J. Sutcliffe, C. Redfield, et al., Structure of hen lysozyme in solution, J. Mol. Biol. 229 (1993) 930–944.
[40] S. Das, S. Pahari, S. Sarmah, et al., Lysozyme-luteolin binding: molecular insights into the complexation process and the inhibitory effects of luteolin towards protein modification, Phys. Chem. Chem. Phys. 21 (2019) 12649–12666.
[41] S. Das, N. Bora, M.A. Rohman, et al., Molecular recognition of bio-active flavonoids quercetin and rutin by bovine hemoglobin: an overview of the binding mechanism, thermodynamics and structural aspects through multi-spectroscopic and molecular dynamics simulation studies, Phys. Chem. Chem. Phys. 20 (2018) 21668–21684.
[42] S. Das, M.A. Rohman, A. Singha Roy, Exploring the non-covalent binding behaviours of 7-hydroxyflavone and 3-hydroxyflavone with hen egg white lysozyme: multi-spectroscopic and molecular docking perspectives, J. Photochem. Photobiol. B Biol. 180 (2018) 25–38.
[43] B. Tu, Z.-F. Chen, Z.-J. Liu, et al., Study of the structure-activity relationship of flavonoids based on their interaction with human serum albumin, RSC Adv. 5 (2015) 73290–73300.
[44] H.L. Yue, Y.J. Hu, J. Chen, et al., Green synthesis and physical characterization of Au nanoparticles and their interaction with bovine serum albumin, Colloids Surf. B Biointerfaces 122 (2014) 107–114.
[45] D.J. Zeeb, B.C. Nelson, K. Albert, et al., Separation and identification of twelve catechins in tea using liquid chromatography/atmospheric pressure chemical ionization-mass spectrometry, Anal. Chem. 72 (2000) 5020–5026.
[46] B.S. Raghavan, S. Kondath, R. Anantanarayanan, et al., Kaempferol mediated synthesis of gold nanoparticles and their cytotoxic effects on MCF-7 cancer cell line, Process Biochem. 50 (2015) 1966–1976.
[47] R. Shukla, N. Chanda, A. Zambre, A. Upendran, et al., Laminin receptor specific therapeutic gold nanoparticles (198 AuNP-EGCg) show efficacy in treating prostate cancer, Proc. Natl. Acad. Sci. U.S.A. 109 (2012) 12426–12431.
[48] A.M. Awwad, N.M. Salem, A.O. Abdeen, Green synthesis of silver nanoparticles using carob leaf extract and its antibacterial activity, Int. J. Ind. Chem. 4 (2013), 29.
[49] E.S. Al-Sheddi, N.N. Farshori, M.M. Al-Oqail, et al., Anticancer potential of green synthesized silver nanoparticles using extract of nepeta deflersiana against human cervical cancer cells (HeLA), Bioinorgan. Chem. Appl. 2018 (2018), 9390784.
[50] S.S. Bag, A. Banerjee, A. Singh, et al., Green synthesis of silver nanoparticle using sechium edule aqueous extract and study of antimicrobial and catalytic activity, Curr. Nanomater. 3 (2019) 140–146.
[51] S. Salatin, S.M. Dizaj, A.Y. Khosroushahi, Effect of the surface modification, size, and shape on cellular uptake of nanoparticles, Cell Biol. Int. 39 (2015) 881–890.
[52] V.S. Radhakrishnan, M.K.R. Mudiam, M. Kumar, et al., Silver nanoparticles induced alterations in multiple cellular targets, which are critical for drug susceptibilities and pathogenicity in fungal pathogen (Candida albicans), Int. J. Nanomed. 13 (2018) 2647–2663.
[53] F. Benyettou, R. Rezgui, F. Ravaux, et al., Synthesis of silver nanoparticles for the dual delivery of doxorubicin and alendronate to cancer cells, J. Mater. Chem. B. 3 (2015) 7237–7245.
[54] D. Wang, D. Kim, C.-H. Shin, et al., Evaluation of epigallocatechin gallate (EGCG) to remove Pb(II) using spectroscopic and quantum chemical calculation method, Environ. Earth Sci. 78 (2019), 138.
[55] R.K. Harwansh, P.K. Mukherjee, A. Kar, et al., Enhancement of photoprotection potential of catechin loaded nanoemulsion gel against UVA induced oxidative stress, J. Photochem. Photobiol. B Biol. 160 (2016) 318–329.
[56] C.S. Robb, S.E. Geldart, J.A. Seelenbinder, et al., Analysis of green tea constituents by HPLC-FTIR, J. Liq. Chromatogr. Relat. Technol. 25 (2002) 787–801.
[57] M.A. Siddiquee, M. ud din Parray, S.H. Mehdi, et al., Green synthesis of silver nanoparticles from Delonix regia leaf extracts: in-vitro cytotoxicity and interaction studies with bovine serum albumin, Mater. Chem. Phys. 242 (2020), 122493.
[58] K.D. Nugent, W.G. Burton, T.K. Slattery, et al., Separation of proteins by reversed-phase high-performance liquid chromatography. II. Optimizing sample pretreatment and mobile phase conditions, J. Chromatogr., A 443 (1988) 381–397.
[59] S. Ashrafpour, T.T. Moghadam, Interaction of silver nanoparticles with Lysozyme: functional and structural investigations, Surfaces and Interfaces 10 (2018) 216–221.
[60] A.S. Sharma, M. Ilanchelian, Comprehensive multispectroscopic analysis on the interaction and corona formation of human serum albumin with gold/silver alloy nanoparticles, J. Phys. Chem. B 119 (2015) 9461–9476.
[61] S. Sen, S. Konar, B. Das, et al., Inhibition of fibrillation of human serum albumin through interaction with chitosan-based biocompatible silver nanoparticles, RSC Adv. 6 (2016) 43104–43115.
[62] N.S. Al-Thabaiti, M.A. Malik, Z. Khan, Protein interactions with silver nanoparticles: green synthesis, and biophysical approach, Int. J. Biol. Macromol. 95 (2017) 421–428.
[63] M.J. Panzner, S.M. Bilinovich, W.J. Youngs, et al., Silver metallation of hen egg white lysozyme: X-ray crystal structure and NMR studies, Chem. Commun. 47 (2011) 12479–12481.
[64] K.S. Ghosh, B.K. Sahoo, S. Dasgupta, Spectrophotometric studies on the interaction between (-)-epigallocatechin gallate and lysozyme, Chem. Phys. Lett. 452 (2008) 193–197.
[65] F. Shen, F. Niu, J. Li, et al., Interactions between tea polyphenol and two kinds

of typical egg white proteins-ovalbumin and lysozyme: effect on the gastrointestinal digestion of both proteins in vitro, Food Res. Int. 59 (2014) 100–107.
[66] J.R. Lakowicz, Principles of Fluorescence Spectroscopy, 3rd ed., Springer, New York, 2006, pp. 27–61.
[67] S.H.D.P. Lacerda, J.J. Park, C. Meuse, et al., Interaction of gold nanoparticles with common human blood proteins, ACS Nano 4 (2010) 365–379.
[68] D.L. Nelson, M.M. Cox, Protein function, in: Lehninger Principles of Biochemistry, 7th ed., W.H. Freeman and Company, New York, 2013, pp. 157–172.
[69] J.B.F. Llyod, Synchronized excitation of fluorescence emission spectra, Nat. Phys. Sci. 231 (1971) 64–65.
[70] C. Barakat, D. Patra, Combining time-resolved fluorescence with synchronous fluorescence spectroscopy to study bovine serum albumin-curcumin complex during unfolding and refolding processes, Luminescence 28 (2013) 149–155.
[71] J.N. Miller, Recent advances in molecular luminescence analysis, Proc. Anal. Div. Chem. Soc. 16 (1979) 203–208.
[72] F. Tanaka, L.S. Forster, P.K. Pal, et al., The circular dichroism of lysozyme, J. Biol. Chem. 250 (1975) 6977–6982.
[73] L. Whitmore, B.A. Wallace, DICHROWEB, an online server for protein secondary structure analyses from circular dichroism spectroscopic data, Nucleic Acids Res. 32 (2004) W668–W673.
[74] S. Roy, Binding behaviors of greenly synthesized silver nanoparticles – lysozyme interaction: spectroscopic approach, J. Mol. Struct. 1154 (2018) 145–151.
[75] S. Roy, S.K. Saxena, S. Mishra, et al., Ecofriendly gold nanoparticles – lysozyme interaction: thermodynamical perspectives, J. Photochem. Photobiol. B Biol. 174 (2017) 284–290.
[76] Z. Aghili, S. Taheri, H.A. Zeinabad, et al., Investigating the interaction of Fe nanoparticles with lysozyme by biophysical and molecular docking studies, PloS One 11 (2016), e0164878.
[77] M. Rai, A. Yadav, A. Gade, Silver nanoparticles as a new generation of antimicrobials, Biotechnol. Adv. 27 (2009) 76–83.
[78] W. Xu, Y. Fan, X. Liu, et al., Catalytic and antibacterial properties of silver nanoparticles green biosynthesized using soluble green tea powder, Mater. Res. Express 5 (2018), 045029.
[79] W.R. Rolim, M.T. Pelegrino, B. de Araújo Lima, et al., Green tea extract mediated biogenic synthesis of silver nanoparticles: characterization, cytotoxicity evaluation and antibacterial activity, Appl. Surf. Sci. 463 (2019) 66–74.
[80] R.A. Hamouda, M.H. Hussein, R.A. Abo-elmagd, et al., Synthesis and biological characterization of silver nanoparticles derived from the cyanobacterium Oscillatoria limnetica, Sci. Rep. 9 (2019), 13071.
[81] S. Shrivastava, T. Bera, A. Roy, et al., Characterization of enhanced antibacterial effects of novel silver nanoparticles, Nanotechnology 18 (2007), 225103.
[82] K. Shivaji, S. Mani, P. Ponmurugan, et al., Green-synthesis-Derived CdS quantum dots using tea leaf extract: antimicrobial, bioimaging, and therapeutic applications in lung cancer cells, ACS Appl. Nano Mater. 1 (2018) 1683–1693.
[83] V.V. Makarov, A.J. Love, O.V. Sinitsyna, et al., "Green" nanotechnologies: synthesis of metal nanoparticles using plants, Acta Naturae 6 (2014) 35–44.